Seismic Behavior of Active Faults Through Multisource Optical Imagery: From Satellite to Drone Resolution (case study: The North Zanjan fault)

Farzaneh Abedi[1], Zohreh Masoumi[1,2], Esmaeil Shabanian[1], Stefano Salvi[3], Stefano Pucci[3]

[1] Department of Earth Sciences, Institute for Advanced Studies in Basic Sciences (IASBS), Zanjan, Iran- farzaneh.abedi7@gmail.com

[2] Center for Research in Climate Change and Global Warming (CRCC), Institute for Advanced Studies in Basic Sciences (IASBS), Zanjan, Iran- z.masoumi@iasbs.ac.ir , shabanian@iasbs.ac.ir

[3] Istituto Nazionale di Geofisica e Vulcanologia, Roma, Italy-stefano.salvi@ingv.it , stefano.pucci@ingv.it

Keywords: Seismic behavior, Optical imagery, Remote sensing, Active tectonics, Tectonic geomorphology, North Zanjan Fault.

Abstract

Detecting and characterizing active faults is crucial for seismic hazard assessment, especially in regions with long earthquake recurrence intervals, such as Iran. Traditional methods, including seismology and geodesy, often fail to identify active faults and assess their seismic potential. This study overcomes these limitations by integrating multi-source datasets with different temporal and spatial resolutions to investigate the North Zanjan Fault (NZF) in the western Alborz Mountains. The NZF is a reverse-dextral fault capable of generating Mw 6.5–7.0 earthquakes. The research employs high-spatial-resolution (HSR) Pleiades Tri-stereo imagery, archival aerial photographs, and RGB overlapping drone-derived imagery to analyze Quaternary geomorphic markers. Photogrammetric techniques are utilized to detect fault traces, map deformed landforms, and reconstruct displacements at multiple scales. By integrating satellite- and archive aerial-derived digital elevation models (DEMs), a detailed 1:5000 scale morpho-structural map is developed, identifying three fault segments connected by thrust fault arrays. Horizontal displacements range from 1.5 to 670 m, while vertical offsets span 1.5 to 77 m. Drone surveys at five locations provide high-resolution data (1:500 scale), revealing an average single-event oblique displacement of 1.10 m. The Sohrein site analysis indicates four Quaternary seismic events, each with an average vertical displacement of 1.30 m. These findings highlight the seismogenic potential of the NZF and demonstrate a scalable methodology for identifying previously unrecognized fault strands, ultimately contributing to improved seismic hazard assessments in the Iranian plateau and similar tectonic environments.

1. Introduction

Detecting and characterizing active faults is a cornerstone of seismic hazard assessment and risk mitigation, particularly in continental regions with long earthquake recurrence intervals, such as Iran. The recurrence time of earthquakes in these regions often spans millennia, posing challenges to traditional methodologies such as seismology, geodesy, and historical seismicity analysis, which frequently fall short in identifying active faults and determining their seismogenic characteristics (Foroutan et al., 2012). Such limitations for the detection of active seismogenic faults result in staggering consequences given by the occurrence of moderate to large destructive earthquakes on the previously unknown faults like the Tabas-e Golshan 1978, Ahar-Varzaghan 2012, and Ezgeleh- Kermanshah 2017 earthquakes. These destructive and unexpected events destroyed or severely damaged vast regions with considerable fatalities.

In fact, during an earthquake, a fault block moves against its counterpart along the fault trace by releasing the elastic energy accumulated around the fault. After the earthquake, the former shape of linear (displaced riverbanks and terrace risers) or planar geomorphic features (alluvial fans) offset along the fault offer valuable insights by preserving evidence of seismic cycles over extended timescales Hence, the scale of the feature used for reconstruction depends on the size of the seismic event and the accuracy of the accessible dataset.

However, these markers are often reworked/smoothed by erosion, necessitating the use of high-resolution topographic data for accurate fault detection and displacement assessment. High-resolution optical and topographic data is essential for detecting fault traces and displaced geomorphic landforms while reducing their uncertainties. Advances in remote sensing and photogrammetric workflows complement traditional active tectonic approaches, enabling more accurate characterization of fault-related deformation and improving our understanding of seismic processes (e.g., Zielke et al., 2015).

The North Zanjan Fault (NZF), a reverse-dextral structure located at the western edge of the Alborz Mountains near Zanjan city, exemplifies these challenges. The fault, with a 60 km recognized length, has no historical or instrumental seismic record, yet possesses the potential to generate moderate to large earthquakes (Solymani Azad et al., 2011), threatening over 550,000 residents in the region. Its geomorphic expression, preserved in Pleistocene and Holocene deposits, provides critical evidence of Quaternary activity. Previous studies (Solymani Azad et al., 2011; Salmanlou, 2014; Badouzadeh, 2018) have characterized the complex structure and the Cenozoic stress evolution of the fault, highlighting its seismogenic potential. Despite these contributions, gaps remain in understanding the detailed segmentation, long-term/single-event displacement patterns, and seismic history of the fault.

This study addresses existing knowledge gaps by employing a multi-scale and multi-temporal remote sensing methodology. The method employs a dual-scale approach: a broad perspective from satellite and aerial data that covers an area of 304 km² and is then complemented by detailed, local-scale drone-surveyed sites in five key areas. The use of archival aerial imagery is particularly significant as it captures landscapes before extensive urbanization and land-use modifications, enabling the identification of geomorphic features that may have been obscured or obliterated in modern settings. This approach revises the previous 1:100,000 geologic map and fault trace, and facilitates the detection of subtle geomorphic markers and systematic offsets, offering a comprehensive understanding of the NZF’s seismogenic behavior. By integrating principles of active tectonics with advanced remote sensing techniques, this research provides a scalable methodology applicable to other poorly characterized faults across continental regions, with low rates of deformation.

2. Study area

The Iranian plateau is deforming due to the Arabian and Eurasia convergence. The total rate of ongoing deformation ranges from 12 to 26 mm/yr across the plateau and surrounding mountain belts such as the Kopeh Dagh, Zagros, and Alborz. This overall rate of deformation is almost a third of the deformation rate reported in the India – Eurasia collision zone and is heterogeneously distributed on numerous crustal faults. Some of these faults form the major boundary of distinct tectonic domains, while other ones are responsible for the accommodation of internal deformation within these domains. These intercontinental faults are characterized by slow rates of slip and normally, long recurrence times of large earthquakes.

The Zanjan region, situated at the margin of the Central Iran and Alborz mountain belt, serves as a remarkable example of an intercontinental setting characterized by a low deformation rate of less than 1 mm per year (Figure 1). The Zanjan region, despite the documented Holocene tectonic activity shaping its landscape, has no record of significant historical or instrumental earthquakes. This seismic silence has consequently been interpreted as evidence of a seismic gap (Solymani Azad et al., 2011). The North Zanjan Fault (NZF), which defines the western boundary of the Alborz mountain belt against the Mianeh - Zanjan depression, spans approximately 60 km and affects Pleistocene and Holocene alluvial geomorphic surfaces and associated drainage systems offering compelling evidence of the recent surface faulting activity of the fault.

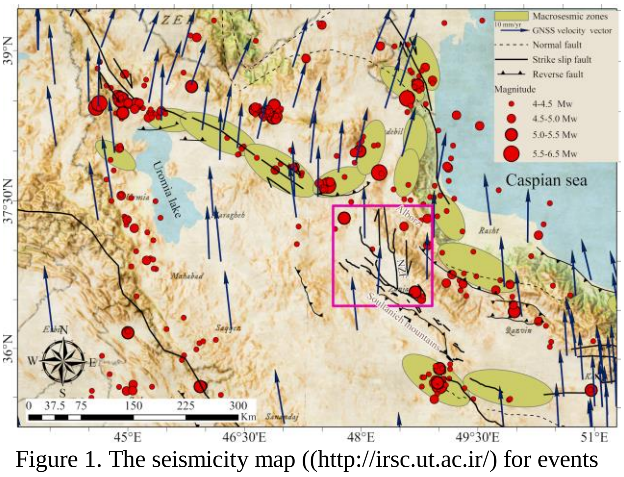

Figure 1. The seismicity map ((http://irsc.ut.ac.ir/) for events M_W>4. The purple square demonstrates the study area. The area of maximum destruction of earthquakes (almost historical) is shown in green ellipses (taken from Solaymani Azad et al., 2015); no specific events affected the Zanjan area. The difference in GNSS velocity vectors estimates a limited range of deformation for the study area (Khorrami et al., 2019).

During the Quaternary, the NZF experienced significant changes in the regional state of stress shifting from a predominantly right-lateral strike-slip mechanism to a reverse fault with a minor right-lateral component (Badouzadeh, 2018; Salmanlou, 2014). The older Paleostress regimes have been active since the Pliocene. The contemporary stress regime has been active since the Holocene and has led to the preservation of geomorphic signatures for both stages of fault activity during the Quaternary. Ignoring this kinematic complexity may result in misinterpretation of geomorphic observations and assessment of the fault behavior. Consequently, high-spatial resolution (HSR) three-dimensional (3D) analyses of Quaternary landforms with different relative ages are essential for deciphering the geomorphic signatures related to distinct periods of fault activity.

3. Method

Moderate to large earthquakes (M_W> 5.5) may rupture the ground surface sufficiently, forming a range of co-seismic features that may be stored in the geomorphology (alluvial terraces, drainage system, and alluvial fans; e.g., Zielke et al., 2015). ‹To investigate co-seismic features of past earthquakes along the NZF, multi-source HSR datasets are utilized. The first part of the research focuses on optical datasets introduction and processing, while the second part is dedicated to fault mapping, morphotectonic map generation reconstruction, measurement, and analysis of geomorphic marker offsets, followed by the interpretation of the results (Figure 2). These drone-surveyed sites, primarily composed of the youngest sediments, are expected to provide valuable insights into recent seismic activity and single-event displacements.

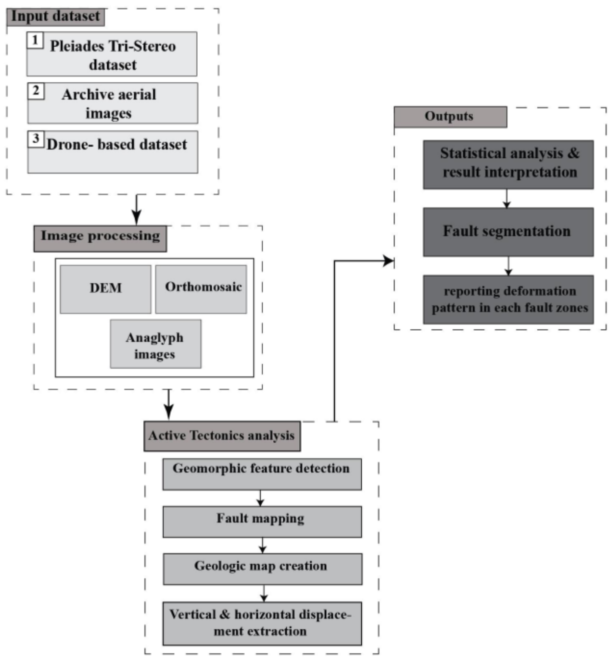

Figure 2. The framework of the study is demonstrated. At the beginning input data including the Tri-stereo Pleiades dataset and (1955-1966) archive aerial images were applied for active tectonic analysis at a general scale. Great-scale studies are conducted on selected key areas also using airborne (drone) optical image acquisitions. Finally, fault-related geomorphic features/landforms were detected and characterized, and the along-strike offset distribution was reconstructed.

3.1. The introduction of optical dataset and photogrammetric processing

Meter-scale Pleiades imagery and 1955–1966 archival aerial-driven DEMs and ortho-mosaics in 304 km^2 are interpreted qualitatively (visual interpretation) and quantitatively (geometric reconstruction) to prepare detailed maps of the fault traces and Quaternary surfaces, and to restore cumulative geomorphic offsets.

The basic theory of using stereo imagery to generate DEM is to match the corresponding points in overlap areas of stereo pairs and then extract the 3D coordinate point clouds. This processing is similar to 3D vision of human eyesight reconstruction. In Tri-

Stereo satellite processing, the relationship between image space and object space can be defined by Rational Polynomial Coefficients (RPCs)(Nasir et al., 2015), enabling a sensor-independent transformation even without GCPs (Ground control points). Conversely, archived imagery and drone-based optical surveys utilize Structure from Motion (SfM) algorithms and GCPs to achieve accurate 3D reconstruction. The photogrammetric processing workflow encompasses feature matching, bundle adjustment, dense matching, rasterization, and ortho-rectification to ensure precise topographic representation (Zhou et al., 2015).

To improve accuracy, five sites for drone-based surveys, characterized by complex structural arrangements, were selected. As an example, the Sohrein site is surveyed (Figure 3) to generate centimeter-scale DEMs that fill critical gaps in spatial detail.

Although satellite and aerial imagery facilitate large-scale coverage in short timeframes, they struggle to accurately represent steep terrains due to nadir-only image acquisition. This limitation arises when multiple surface slopes are present, leading to incomplete or distorted terrain representation. Drones, however, capture images from multiple angles (convergent views) and perform cross-flight missions, even in nadir orientation, effectively reducing topographic distortions.

Unlike satellite-derived datasets such as Google Earth, Bing, or SAS Planet, which rely on images acquired from satellites or airborne platforms, drone-surveyed imagery provides superior spatial resolution, optimized mapping scales, and adaptable flight patterns. These advantages facilitate the precise mapping of geologic exposures and outcrops, allowing for controlled vertical distances, orientations, and image overlaps. This flexibility makes drone photogrammetry particularly useful for active fault investigations, where high-resolution topographic data is essential for analyzing surface deformations and structural features.

This site, which is situated 21 km northward of Zanjan City and west of Sohrein Village, focuses on the intersection area of the NZF and the Sohrein seasonal river, where several river terraces were formed. This site was surveyed using a PPK-based platform and fly conducted on the DEM. The 117 ha area survey in 2 days and 7 missions. It is noteworthy, that researchers spend one day on GCP establishment and Real-Time Kinematic (RTK) surveying. (details in Table 1).

Table 1. The data specification of the Sohrein UAV site.

Aerial photogrammetric camera	Mavic II pro-PPK
Focal length (mm)	10
flight height (m)	100
Number of photographs	2545
Number of missions	7
Overlap	85% (in length)-75% (in width)
Ground spatial distance (GSD) (cm)	2.5
Covered area (ha)	117
Format type	.jpg
ISO	100
f-stop	4.5-6.3
Shutter speed	1:1000
The horizontal speed of the platform (m/s)	6
Number of base stations	4
Number of GCPs	9
Number of checkpoints	11

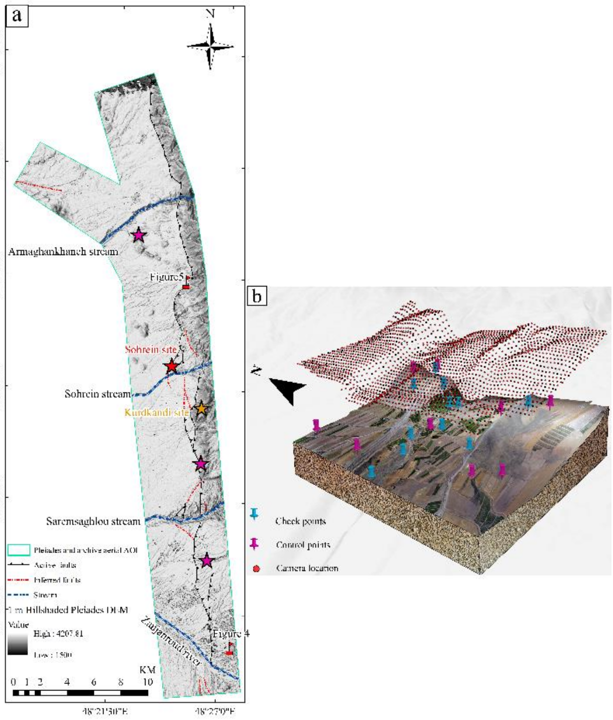

Figure 3. a) The 1m shaded relief of the Pleiades DEM covers 304 km^2. The drone surveys are shown by stars, the red one demonstrates the location of the Sohrein site. The black lines are certain Quaternary faults and the red lines are inferred faults (Solymani Azad et al., 2011). b) A 3D view of the Sohrein drone site and the location of GCPs is shown. Pink markers are control points to transfer the model into the real-world coordinate system. Blue markers are checkpoints and validate the quality of the final DEM.

3.2. The active tectonic principles

Here, fault mapping, Quaternary morphotectonic map generation, and both vertical/horizontal principles of displacement reconstruction are explained.

3.2.1. Mapping of fault traces and Quaternary geomorphic units

Fault mapping relies on 3D visual interpretation of lithological disruptions, junctions, fracture traces, outcrop boundaries, stream configurations, and abrupt drainage pattern changes. Various DEM visualization techniques, including Red Relief Image Map (RRIM) hill-shaded DEMs, and contour lines, enhance terrain analysis by emphasizing topographic variations and structural discontinuities. Ortho-mosaics provide color differentiation and shadow orientation, aiding in the interpretation of landform relationships, while anaglyph visualization offers real 3D perception, even in historical imagery from 1955–1966. To ensure accuracy, expert interpretations and field observations are integrated. Fault traces are classified into three categories—certain, inferred, and suspected—based on geological and geomorphic factors such as land units (e.g., vegetation, scarps, hills) and land elements (e.g., crest, hillside, or foot slope of a scarp).

Additionally, geomorphic mapping distinguishes areas with similar physical features and terrain attributes, including alluvial fans, texture, roughness, incision severity, location, topography, soil, and lithology. Finally, each category displays distinct units, reflected in variations in color on orthomosaics and patterns on hill-shaded DEMs. Older surfaces tend to show smoother topography and higher incision levels, indicative of prolonged drainage network activity.

3.2.2. The fault segmentation

Fault segmentation models are useful to predict the maximum magnitude of future seismic events. These models apply several sources of information about faults such as geometrical complexities (fault strike, length, step-over properties), tectonically controlled Quaternary deposit/erosional distribution, and geophysical (kinematics). In addition, fault segmentation is pursued through displacement measurements analysis for each segment to explore potential correlations between structural and behavioral segmentations.

3.2.3. The horizontal displacement

To rebuild the geometry of a feature that is laterally displaced, one can perform a retro deformation by realigning the correspondent geomorphic elements on the two sides of the fault and matching the cutoffs. The seamless orthomosaic is set as the base map and piercing lines are projected on the fault plane. For example in a stream channel, the streambed, and both the left and right banks are considered. In ideal conditions, three different values (max, optimum, and min) can be recorded (Figure 3), in this way the range of displacement is set. In this way, the a±b includes "a" as the average displacement value, and "b" is the distance from the average which is completely different from stvd in arithmetic.

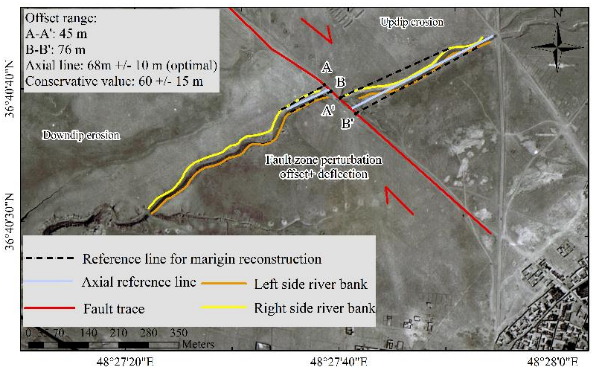

Figure 4. Geometric reconstruction of the displaced stream channel shows 68±10 m lateral movement. The active faults are in red and piercing lines are in black. The 1966 orthomosaic is set as the background. Figure 3 demonstrates the location of this feature along the NZF.

3.2.4.The vertical displacement

The vertical retro-deformation measurements of surface-breaking earthquakes are performed using DEM. Extracted strike-perpendicular profiles were examined for identification of the scarp base and scarp top portions. To estimate the height of a scarp, it is necessary to fit piercing lines on the footwall (FW) and hanging wall (HW). According to Figure 5, the separation of these piercing lines (light blue and red) represents the vertical offset. Local topographic perturbation, the slight erosion or collapse of the HW/FW by surface process or human activities have an undeniable effect on the quality of reconstruction.

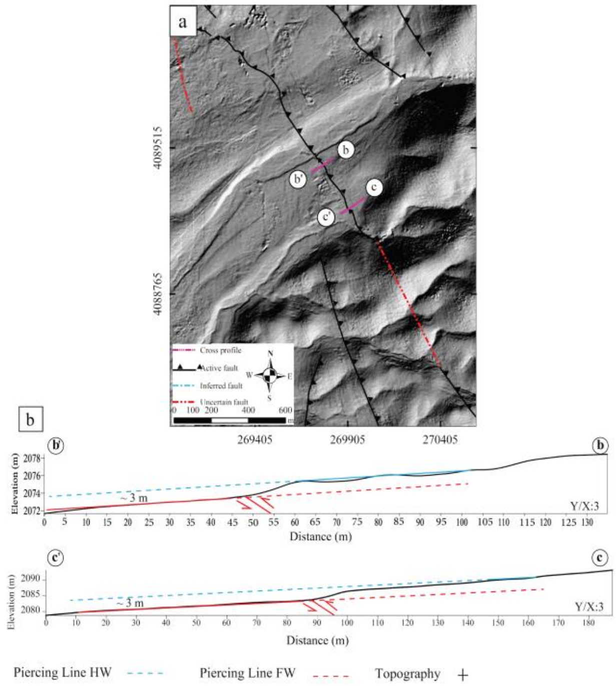

Figure 5. The study site is located in the south of Vannanaq village. a) bb' and cc' cross profiles cross through one fault strand. b) The reconstruction of bb' and cc' shows approximately 3 m vertical offset. The scale ratio of the vertical to horizontal axis is 1:3. Figure 3 demonstrates the location of this feature along the NZF.

4. Results and discussion

Advancements in the spatial resolution remotely sensed datasets (e.g.: DEM and orthophotos) transformed active tectonics from qualitative to a more and more quantitative one in 100 years. The accuracy of the generated DEM depends on various factors, including the spatial and radiometric resolution of input data, the method of photo acquisition, as well as the topography and surface texture of the study area.

Comparative analysis reveals that archive aerial and Pleiades DEMs provide higher efficiency in fault detection than the freely available 30 m SRTM DEM. In the 1955 DEM, landform features and erosion depths are more distinguishable than in the 30 m SRTM DEM. However, both the 1955 and 1966 DEMs contain artifacts resulting from poor illumination and suboptimal image exposure, particularly when compared to the Pleiades DEM. Despite these limitations, they remain valuable for visual feature inspection, especially in regions undergoing significant landscape modifications.

In fact, for reconstructing vertical displacements, cross-profiles extracted from the Pleiades DEM exhibit less noise, enhancing measurement precision. Notably, the cm-resolution drone-based DEM captures significantly higher detail. While drone photogrammetry provides a 1:500 map that introduces more precise fault trace mapping, its limited spatial coverage restricts its applicability to large-scale studies. The total error (both planimetric and vertical) of the generated cm DEM evaluated using 11 checkpoints is better than 7 cm. This optimum output is the result of the PPK data capturing and flying on the DEM which strengthens the photogrammetric block and supports the designed overlap parameter and GSD during the flight.

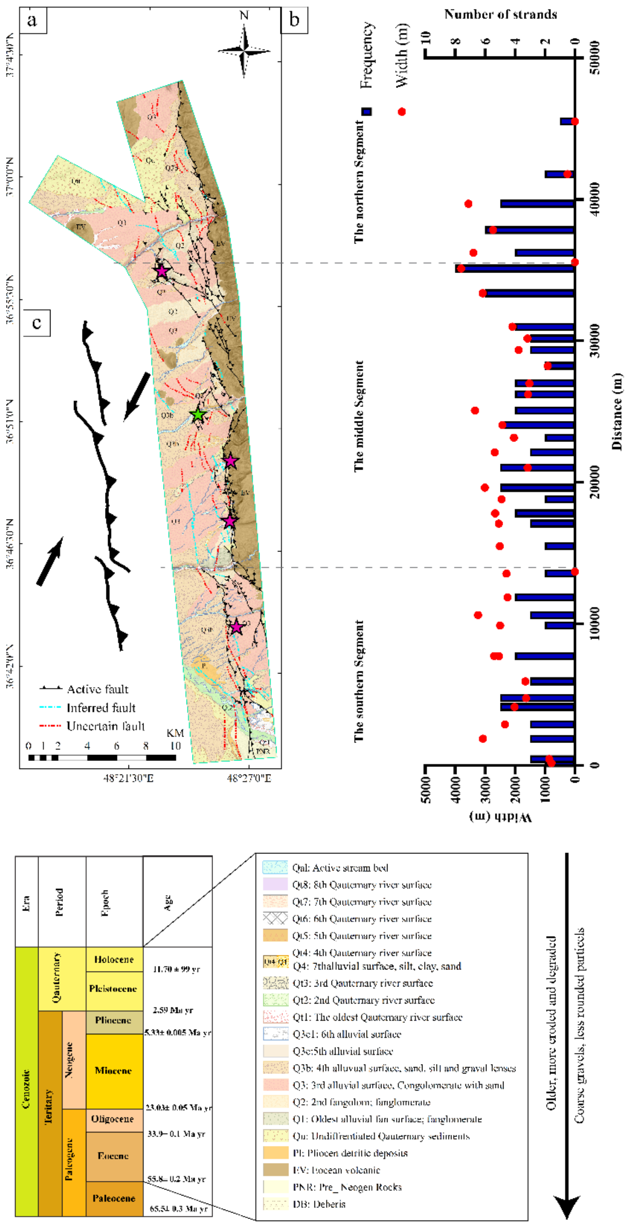

Figure 6. a) The geologic map indicates fluvial terraces and alluvial fans in 8 and 7 categories based on color, roughness, texture, and relative location. As the readers look downward geomorphic units become older and experience more degradation and erosion. The fault map is grouped into three valid groups: active, inferred, and uncertain. The drone survey showed the shape of stars, the red one demonstrates the location of Figure 3. b)The number of strands and weak zone width along the NZF are displayed. c) The rose diagram of the strike of fault strands is dominantly north to south. c) The simple sketch of three segments from south to north. The NE-SW orientation of modern stress regime and structural alignments causes thrust faulting in relay zones.

The available maps of the NZF were limited to small scales (1:250,000 to 1:100,000) that only provided the general geometry of the fault. Using HSR remote sensing datasets and field visits, we prepared a fault trace map and morpho-structural map at a scale better than 1:5000 (Figure 6(a)). Geomorphic surfaces associated with fluvial terraces and alluvial fans are grouped into 8 and 7 categories, respectively, according to their relative forming sequences(Figure 6(a)).

Based on this updated map, the NZF zone can be classified into three main segments (Figures 6(c)) with NS orientation, each rotating to the NW at its northern end. Each segment is connected with overlapping areas covered by arrays of thrust faults(Figures 7, and 8). The southern segment is traceable from the southern flanks of Soltanieh mountain to the left-hand of the Saremsaghlou stream. The middle segment begins in the east of the southern. The 3.30 km length of the first relay zone transfers the displacement from the southern segment to the middle segment and continues to the north. The northern segment passes the margin of the mountain and plain on the northern banks of the Armaghankhaneh stream and fades after 16 km. The 3.8 km overlapping length at the second step over involves 12% length of the middle segment. As shown in Figure 6(b), the middle segment exhibits the smallest variation in width and the number of detected strands, whereas the northern segment has the simplest structural arrangement.

The southern segment, the youngest, shows fault existence from east to west and spans 14.40 km with a 344° orientation, extending from the Soltanieh Fault southwest of Zanjan to the Saremsaghlou stream. The middle segment, located 2.36 km north of the southern segment, is connected via a relay zone with thrust arrays. These thrusts, over 3.30 km with a 324° azimuth, transfer displacement between the southern and middle segments. The northern segment follows the mountain fronts, covering a distance of 16.20 km. This segment exhibits relatively lower structural complexity, primarily aligning along the boundary between the mountain and the plain. As the middle segment diminishes, the northern segment shifts eastward by approximately 3.15 km. The second stepover, with an overlapping length of 3.8 km, accounts for 12% of the middle segment's total length. Above the Armaghankhaneh stream, evidence of westward fault migration becomes minimal, resulting in a narrower deformation zone.
Remote sensing observations reveal 99 systematic dextral displacements along the mountain/pediment contact. Additionally, the presence of multiple parallel splays of linear fault scarps forms a wide deformation zone ranging from 500 m to 4 km from the main fault trend. The observed linear trends and Quaternary scarps are indicative of almost 41 cumulative vertical displacements.

4.1. The horizontal displacement distribution

Variations in the trend of displacement values considering geomorphic formation sequence along the fault provide insights into stages of structural evolution and slip history (Klinger et al., 2011). The cumulative horizontal displacements measured in the Q_2 (670 ± 50 m), Q_3 (410 ± 40 m), and Q_{3b} (102 ± 3 m) units shown in Figure 7 exhibit a consistent displacement distribution pattern across all three fault segments. Notably, the dislocation affecting coeval deposits presents values with the same order of magnitude, suggesting a similar along-strike distribution of the long-term slip rate in the hypothesis of the same faulting onset. A similar trend is also observed for the Holocene cumulative offsets, although we have limited observations. The maximum value for Holocene cumulative offsets in the middle and northern segments is 12.0 ± 1.0 m. However, in the southern segment, only one geomorphic marker with an offset of approximately 4 m (located on the upper side of the Zanjan-Armaghankhaneh road) was identified. This discrepancy may be attributed to recent sedimentation processes in the southern segment, which could have obscured evidence of maximum cumulative Holocene seismic activity.

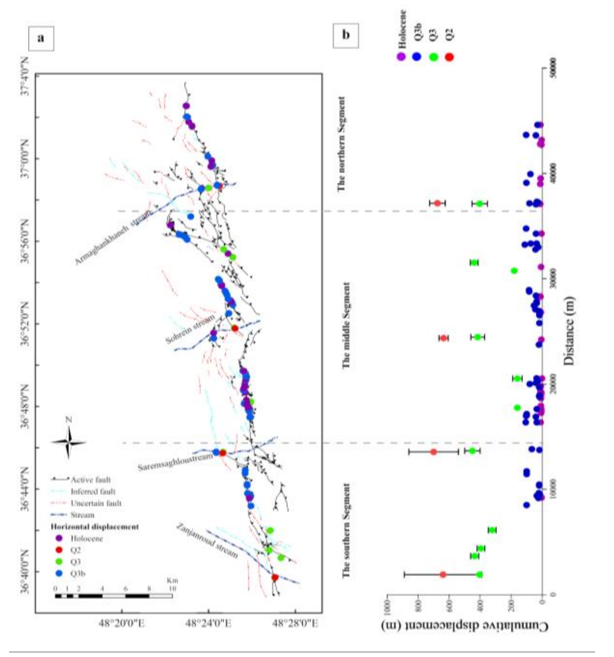

Figure 7. The NZF horizontal displacements (circles). The locati of displaced geomorphic features is related to a desired reference the south of Zanjan city. a) Sketch of the fault system with distribution cumulative location of the horizontal displacements. Along-strike distribution curve of the horizontal displacements

4.2.The vertical displacement distribution

Cumulative vertical displacement shows the same pattern as the horizontal displacement trend. The maximum cumulative vertical offset Q_3(77.00±7.00 m) is measured only in the middle segment caused by Q3b sedimentation in the footwall of the southern and northern segments. The maximum cumulative vertical offset Q_{3b} (34.00±3.00 m) and Holocene (1.50±1.00 m) cumulative displacement were observed in all three segments (Figure 8).

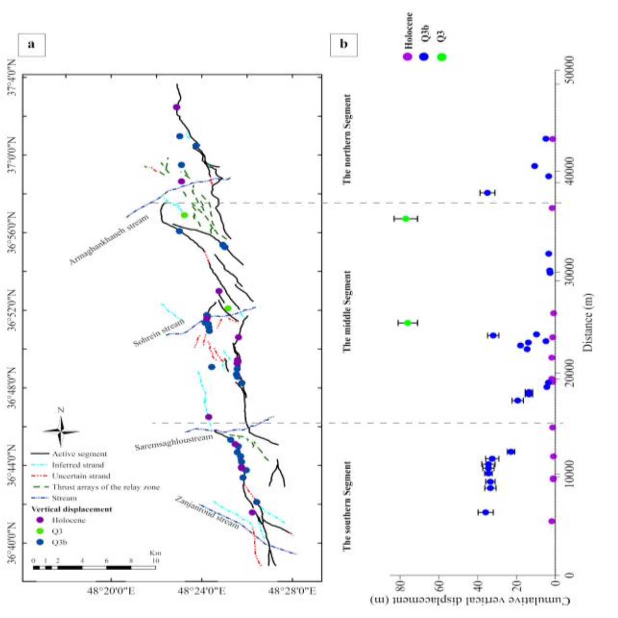

Figure 8. The NZF vertical displacements (circles). The location of displaced geomorphic features is related to a desired reference at the south of Zanjan city. a) Sketch of the fault system with distribution cumulative location of the vertical displacements. b) Along-strike distribution curve of the vertical displacements.

4.3. The site scale findings

Large-scale observations in Kurdkandi site (Figure 3) reveal an average oblique single-event displacement of 1.10 m. As an example, the Sohrein site (Figure 9) shows an interesting pattern of uplifting, where scarps and asymmetrical and uplifted river terraces are manifestations of reverse faulting in young geomorphic surfaces. A flight of eight fluvial terraces (Q_{t1}, …, Q_{t8}) can be distinguished progressively inset along the Sohrein stream channel. The asymmetrical configuration of the terraces and the distinctive change in the width of the active bed are the signatures of active reverse faulting. Reverse faulting often causes tilting of terraces, where older terraces are more deformed than younger ones, indicating progressive uplift over time (Bull, 2007). In the knick points of the active bed lateral incision substitutes with depth incision, so the width of the stream changes in the vicinity of the fault trace.

The Sohrein site is an interesting appearance of seismic activity in the recent stress regime, scarps and river terraces are manifestations of reverse faulting in young geomorphic surfaces. This site is located in the west of Sohrein village. The Sohrein seasonal stream flows westwards across the fault zone. Evident human-induced landscape modifications are the result of intense agricultural activities.

The general trend of faulting is NS at the mountain-plain boundary, yet at the vicinity of the Sohrein village, it turns somehow to the west. While carrying out fault identification, fault strand parallelization is an outstanding point that is in line with the reverse faulting properties. The length of fault strands is limited; the multiplicity of the strands illustrates the width of the weakness zone. The longest strand crosses the stream and it is obvious at the foothill in the upper stream bank. The telecommunication equipment is placed on an elevated hill, which overlooks the western plain at 1859 m height. The elevation difference between the mountainous area and the plain may reach 60 m. In this way, the high elevated topography is located at the hanging wall and the lowland plain is situated in the footwall. Except for the eastern hills of this area, the whole area does not show much slope change.

Several young strands were not visible in primary input data (Satellite and archive aerial imageries), using drone-derived photogrammetric outputs regional map updated. The young strands are distributed in early river terraces. Some of them are identified in the boundary of two different terraces, and others are disturbed in the same-age terrace.

To reconstruct the vertical displacement preserved in the Sohrein fluvial stream, two fault-parallel profiles are selected (Fig. 9). Sequential decreases in vertical offset amounts are proportional to the relative age of the offset terraces such that, the older the trace, the larger the amount of vertical offset (e.g., Q3b offset value of ~5.50 m compared to Q_{t7} offset value of ~1.70 m) (Figure 9 and Table 2). The right-hand terrace (Q_{t7}) and the left-hand terraces (Q_{t6}, Q_{t7}, Q_{t8}) of the Sohrein stream have been deformed simultaneously by the most recent seismic activity. Differentiating vertical offsets across surfaces of various ages reveals evidence of four Quaternary single events, each with an average vertical displacement of approximately 1.30 m (Table 2). The oldest seismic event(s) in this site is younger than the Q_{3b} terrace. Then another seismic event happened after Q_{t2} formation. Subsequently, Q_{t3}, …, Q_{t4} emerged and then interrupted by another seismic event(s), this event(s) is younger than Q_{t4}. Finally, after the configuration of Q_{t5}, …, Q_{t8} the latest seismic event printed its evidence on this fluvial set.

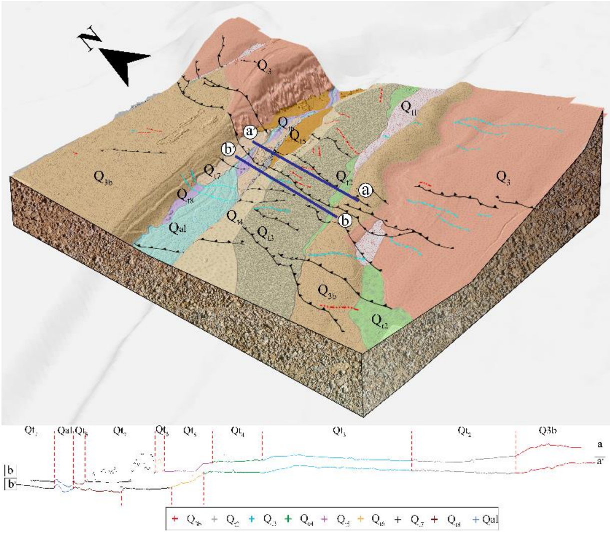

Figure 9. (a) Block diagram of the Sohrein fluvial stream. Several fluvial terraces are displaced vertically by reverse faulting; (b) The fault-parallel profiles in the footwall and hanging wall are presented.

Table 2. The vertical displacement interpretation of the drone-surveyed site

Surface	vertical displacement (m)	Mean vertical displacement (m)	Displacement difference (m)
Q_{3b}	Average: 5.50±0.25 m	5.50±0.25 m	1.20±0.40 m
Q_{t2}	Average: 4.30±0.30 m	4.30±0.30 m	
Q_{t3}	Average: 3.00±0.20 m	3.10±0.25 m	1.25±0.40 m
Q_{t4}	Average: 3.15±0.15 m		
Q_{t6}	Average: 1.60±0.15 m	1.70±0.30 m	1.40±0.45 m
Q_{t7}- left hand	Average: 1.75±0.15 m		
Q_{t8}- left hand	Average: 1.80±0.15 m		
Q_{t7}- right hand	Average: 1.65±0.15 m		

4.4. Discussion

Regarding the broad-scale analysis: the maximum cumulative horizontal displacement ranges between 1.5 and 670 m, and the vertical displacement between 1.5 and 77 m. Finding the same amount of cumulative displacement in each segment shows that the fault behaves similarly in each segment during its long-term activity. The large strike-slip displacements are related to the time (Pleistocene) when the maximum regional pressure had a near NS orientation (refer to Salmanlou, 2014 and Baduzadeh, 2017). The last stress regime with maximum NE compression has been started in the Pleistocene and is active till now. This stress regime is responsible for the youngest reverse faulting in the Zanjan area.

No displacements were detected in the Q_1 unit, possibly due to surface degradation processes such as erosion or burial by recent deposits. Furthermore, an analysis of the maximum cumulative horizontal and vertical slip indicates a relatively uniform slip distribution from south to north. There is no structural and geomorphic evidence to suggest that the NZF terminates at the northern end of the northern segment; rather, its traceability in the mountain becomes complicated. In contrast, in the southern segment, the NZF interacts with the Soltanieh Fault, where deformation manifests as reverse faulting. Within the study area, no significant decrease in displacement (i.e. slip deficits) is observed at geometrical complexities (e.g. step-overs) suggesting the presence of an efficient segment boundary (i.e. barrier to rupture propagation). The relatively uniform displacement amounts across all three segments indicate a hard linkage bypassing these geometrical complexities.

Recent optical drone surveys have documented seismic deformations affecting geomorphic markers within nascent landforms. Given the limited frequency and amplitude of these displacements, high-resolution, centimeter-scale investigations are essential for advancing active tectonic studies.

5. Conclusion

This study employs high-resolution Pleiades satellite imagery, archival aerial photographs, and drone surveys to analyze fault activity at both regional and site-specific scales. The broad-scale analysis provides insights into fault arrangement and cumulative displacements, while detailed site-scale investigations using drone surveys refine fault mapping and enable the detection of single-event displacement.

The 1-m DEM and orthomosaic provided the 1:5000 scale morpho-structural map of the NZF, detecting three fault segments linked by thrust fault arrays in overlapping relay zones. 91 observed horizontal displacements range from 1.5 to 670 m, while 41 vertical offsets span 1.5 to 77 m along fault strike. The cumulative offsets of geomorphic markers indicate similar trends along all three segments suggesting that structural segmentation is not an obstacle for a similar seismogenic behavior of the fault segments. The discrepancy between strike-slip and vertical displacement be explained by diachronous older strike-slip and younger reverse kinematics of the fault due to the prevalence of different stress regimes during the fault history. To investigate the latest seismic activity of the fault, several drone-based sites were selected, based on the young sedimentary cover and structural complexity. In this way, the number of reliable observations at the local scale increased and the prepared geomorphic maps were edited and updated to 1:500 scale. The centimetric DEM and orthomosaic revealed an average 1.10 m single-event oblique displacement. The Sohrein fluvial system is an example of sequential vertical displacement, at least four seismic events can be distinguished, each with an average vertical displacement of approximately 1.30 m.

The NZF is a seismic fault and according to the available evidence, it can cause large earthquakes with a magnitude of 6.7 to 7 MW. By adding dating experiments on identified Quaternary surfaces, the results of this research can be applied to slip rate estimation of the NZF. Likewise, determination of the seismic behavior of the NZF becomes possible if paleo-seismological research is performed accurately.

These findings offer critical insights into the seismogenic potential of the NZF and present a methodological framework applicable to other unrecognized faults on the Iranian Plateau, contributing to improved regional seismic hazard assessment.

Acknowledgments

This study was conducted with the support of the European Space Agency (ESA) through the approval of an educational proposal. F.A. is deeply grateful to Dr. Riccardo Civico for his invaluable guidance during her visit to INGV. Our appreciation also goes to the Natural Resource Organization of Zanjan Province for granting access to the 1955–1966 archival aerial imagery.

References

Badouzadeh, M., 2018: Active tectonics and segmentation of the North Zanjan fault, Department of Earth Sciences, MSc thesis, Institute for Advanced Studies in Basic Sciences (IASBS), Zanjan, Iran.

Foroutan, M., Sébrier, M., Nazari, H., Meyer, B., Fattahi, M., Rashidi, A., Le Dortz, K., & Bateman, M. D., 2012: New evidence for large earthquakes on the Central Iran plateau: *Palaeoseismology of the Anar fault. Geophysical Journal International*, 189(1), 6–18. doi.org/10.1111/j.1365-246X.2012.05365.x

Khorrami, F., Vernant, P., Masson, F., Nilfouroushan, F., Mousavi, Z., Nankali, H., Saadat, S. A., Walpersdorf, A., Hosseini, S., Tavakoli, P., Aghamohammadi, A., & Alijanzade, M., 2019: An up-to-date crustal deformation map of Iran using integrated campaign mode and permanent GPS velocities. *Geophysical Journal International*, 217(2), 832–843. doi.org/10.1093/gji/ggz045.

Salmanlou, A., 2014: Investigating changes in late Cenozoic stress field (Miocene-Quaternary) in Zanjan area and its application in geodynamics Northwest of Iran. MSc thesis, BASU, Hamedan, Iran.

Solaymani Azad, S., Dominguez, S., Philip, H., Hessami, K., Forutan, M., Zadeh, M. S., & Ritz, J., 2011: Tectonophysics The Zandjan fault system : Morphological and tectonic evidence of a new active fault network in the NW of Iran. *Tectonophysics*, 506, 73–85. doi.org/10.1016/j.tecto.2011.04.012

Solaymani Azad, S., Philip, H., Dominguez, S., Hessami, K., Shahpasandzadeh, M., Foroutan, M., Tabassi, H., & Lamothe, M., 2015: Paleoseismological and morphological evidence of slip rate variations along the North Tabriz fault (NW Iran). *Tectonophysics*, 640–641, 20–38 doi.org/10.1016/j.tecto.2014.11.010

Zielke, O., Klinger, Y., & Arrowsmith, J. R., 2015: Fault slip and earthquake recurrence along strike-slip faults - Contributions of high-resolution geomorphic data. *Tectonophysics*, 638(1), 43–62. doi.org/10.1016/j.tecto.2014.11.004

Zhou, Y., Parsons, B., Elliott, J. R., Barisin, I., & Walker, R. T., 2015: Assessing the ability of Pleiades stereo imagery to determine height changes in earthquakes: A case study for the El Mayor-Cucapah epicentral area. *Journal of Geophysical Research: Solid Earth*, *120*(12), 8793–8808. doi.org/10.1002/2015JB012358.